We are IntechOpen, the world's leading publisher of Open Access books Built by scientists, for scientists

4,800
Open access books available

122,000
International authors and editors

135M
Downloads

Our authors are among the

154
Countries delivered to

TOP 1%
most cited scientists

12.2%
Contributors from top 500 universities

CLARIVATE ANALYTICS BOOK CITATION INDEX INDEXED

WEB OF SCIENCE™

Selection of our books indexed in the Book Citation Index in Web of Science™ Core Collection (BKCI)

Interested in publishing with us?
Contact book.department@intechopen.com

Numbers displayed above are based on latest data collected.
For more information visit www.intechopen.com

Higher Dimensional Spatial Expression of Upper Limb Manipulation Ability based on Human Joint Torque Characteristics

Makoto Sasaki[1], Takehiro Iwami[2], Kazuto Miyawaki[3],
Ikuro Sato[4], Goro Obinata[5] and Ashish Dutta[6]
[1]Iwate University, [2]Akita University, [3]Akita National College of Technology
[4]Miyagi Cancer Center Research Institute, [5]Nagoya University
[6]Indian Institute of Technology Kanpur
[1-5] Japan, [6]India

1. Introduction

A basic ergonomic approach to biomechanical analysis of the human body for using assistive devises considers the individual's body functions, his physical load and the efficiency of the assistive devices. Biomechanical analysis using a rigid link model and the musculoskeletal model is a more objective technique. It replaces electromyogram analysis, and has been applied for the estimation of joint forces and torques, muscular tensions, and energy consumption during the use of various devices such as wheelchairs and assistive carts (Sasaki et al., 2005, 2008; Miyawaki et al., 2000, 2007). In this case both the simultaneous measurements of the external forces acting on a human body and the body movements are required for the analysis. On the other hand, analytical tools using computer generated mannequins, which need no measurement data of human motion, have also been developed (Jack; Siemens PLM Software and RAMSIS; Human Solution GmbH and Safework; Safework Inc., etc.). A computer generated mannequin––with standard body characteristics such as length, weight and joint range of motion––is useful for evaluating the compatibility of humans and different industrial products from the viewpoints of the workplace, work posture and also for reducing related design time and development costs. However, it is very difficult to standardize the body characteristics of elderly or physically handicapped people. Especially, the body functions and muscle characteristics of people with spinal cord injuries differ strikingly from those of normal people, depending on the lesion level and extent of paralysis. Therefore, accurate evaluation of an individual's proper body functions and development of assistive devices based on such evaluations are indispensable.

In order to quantify an individual's body functions, the concept of manipulability (Yoshikawa, 1984, 1985, 1990) that is used to analyze robot manipulators, was applied to evaluate the manipulability of the upper and lower limbs (Ohta et al., 1998; Hamada et al., 2000). All possible velocities, accelerations, and forces at the end-effector can be represented

as ellipsoids or polyhedra using the concept of manipulability. This evaluation method, which is commonly used in the field of robotics, provides effective knowledge for evaluation of the manipulability of upper and lower limbs considering both the kinematics and dynamics of the system.

However, this evaluation method is based on the assumption that the torque characteristic of a human joint is constant, and is hence not very accurate because the maximum torque generated at a human joint varies with the joint angle and direction of rotation. Moreover, although the manipulability of the upper and lower limbs in three-dimensional space is expressed as a six-dimensional hyperellipsoid at the maximum, it is difficult to imagine an ellipsoid in four or more dimensions. Even in the field of robotics, the visualization method of a higher-dimensional hyperellipsoid defined in a space with dimensions equal to the degrees of freedom of a hand, has not been clarified yet. A slack variable is generally introduced to search for the vertex of the polytope (Shim & Yoon, 1997; Chiacchio et al., 1997; Lee, 2001). It is extremely difficult to search for the region of a higher-dimensional polytope accurately using these methods because of its huge computational complexity, and it is also difficult to formulate an objective function in the case of linear programming.

In this chapter, we present a manipulating force ellipsoid and polytope reflecting an individual's joint torque characteristics as a new evaluation method for assessing the manipulability of an upper limb. We also present a visualization algorithm for a higher dimensional hyperellipsoid and a vertex search algorithm for a higher-dimensional polytope. As a practical application of the proposed methods, we also introduce a wheelchair adaptation problem. These methods, which were mainly developed to evaluate the upper limb manipulability, are also applicable to analyze a robot manipulator's manipulation capabilities.

2. Seven Degree of Freedom Upper-Limb Model

Figure 1 portrays a seven DOF-rigid-link model of the upper limb. In the model, θ_1, θ_2, and θ_3 represents the shoulder flexion(+)/extension(-), adduction(+)/abduction(-), and external rotation(+)/internal rotation(-) respectively. In addition, θ_4 is elbow flexion(+)/extension(-); θ_5, θ_6, θ_7 signify wrist supination(+)/pronation(-), palmar flexion(+)/dorsiflexion(-), and radial flexion(+)/ulnar flexion(-) respectively. The physical parameters of each link, e.g., mass, center of gravity, inertia matrix, are calculated using regression equations based on the body weight and link length (Ae et al., 1992). In general, the dynamic equation of motion of the upper limb is given as

$$\boldsymbol{\tau} = \boldsymbol{M}(\boldsymbol{\theta})\ddot{\boldsymbol{\theta}} + \boldsymbol{h}(\boldsymbol{\theta},\dot{\boldsymbol{\theta}}) + \boldsymbol{g}(\boldsymbol{\theta}) + \boldsymbol{J}^T\boldsymbol{F}\,, \tag{1}$$

where $\boldsymbol{\tau} \in \boldsymbol{R}^l$ is a joint torque vector, $\boldsymbol{\theta} \in \boldsymbol{R}^l$ is a joint angle vector, $\boldsymbol{M}(\boldsymbol{\theta}) \in \boldsymbol{R}^{l\times l}$ is an inertia matrix, $\boldsymbol{h}(\boldsymbol{\theta},\dot{\boldsymbol{\theta}}) \in \boldsymbol{R}^l$ are centrifugal and Coriolis terms, $\boldsymbol{g}(\boldsymbol{\theta}) \in \boldsymbol{R}^l$ is a gravity term, $\boldsymbol{J} \in \boldsymbol{R}^{n\times l}$ is a Jacobian matrix, $\boldsymbol{F} \in \boldsymbol{R}^n$ is a hand force vector, $l\,(=7)$ is the number of joints, and $n\,(n \le 6)$ represents the degrees of freedom of the hand. Because the net joint torque for generating the hand force can be written as

$$\tilde{\boldsymbol{\tau}} = \boldsymbol{\tau} - \boldsymbol{M}(\boldsymbol{\theta})\ddot{\boldsymbol{\theta}} - \boldsymbol{h}(\boldsymbol{\theta},\dot{\boldsymbol{\theta}}) - \boldsymbol{g}(\boldsymbol{\theta})\,, \tag{2}$$

the relation between the joint torque and the hand force is given as

$$\tilde{\boldsymbol{\tau}} = \boldsymbol{J}^T \boldsymbol{F} \,. \tag{3}$$

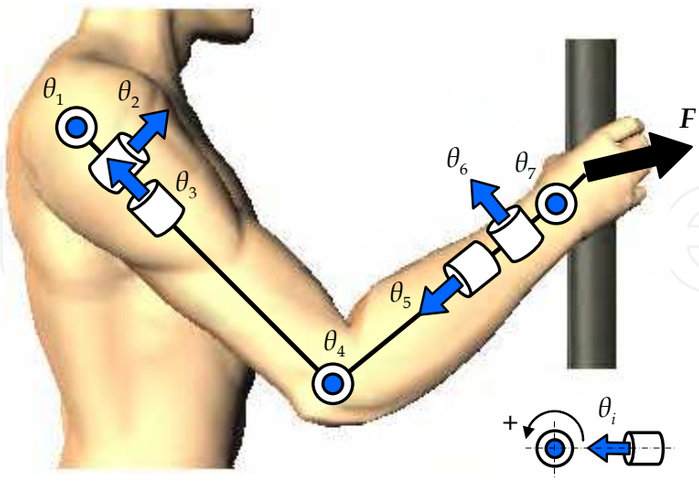

Fig. 1. Seven-rigid-link model of the upper limb.

This equation means that an individual's hand force characteristic is obtained by substituting measurable joint torque characteristics into $\boldsymbol{\tau}$. Because the joint torque characteristics vary according to the joint angle and direction of rotation, the maximum joint torque that can be generated at an arbitrary condition is given as

$$\tilde{\tau}_{imax} = \tau_{imax}(\theta_i) - M_i(\boldsymbol{\theta})\ddot{\boldsymbol{\theta}} - h_i(\boldsymbol{\theta}, \dot{\boldsymbol{\theta}}) - g_i(\boldsymbol{\theta}) \tag{4}$$

$$\tilde{\tau}_{imin} = \tau_{imin}(\theta_i) - M_i(\boldsymbol{\theta})\ddot{\boldsymbol{\theta}} - h_i(\boldsymbol{\theta}, \dot{\boldsymbol{\theta}}) - g_i(\boldsymbol{\theta}) \,, \tag{5}$$

where $\tau_{imax}(\theta_i)$ and $\tau_{imin}(\theta_i)$ signify the maximum joint torque that can be generated at joint angle θ_i in a positive direction or a negative direction, and $i\ (=1,2,\cdots,l)$ is the joint number. These joint torques can be quantified using a Cybex (Cybex Inc.) or Biodex machine (Medical Systems Inc.). Therefore, all the possible hand forces in a daily life motion is given by joint torque that satisfies the following conditions.

$$\tilde{\tau}_{imin} \le \tilde{\tau}_i \le \tilde{\tau}_{imax} \tag{6}$$

3. Manipulating Force Ellipsoid Considering Joint Torque Characteristics

3.1 Derivation of the Ellipsoid

The manipulating force ellipsoid presents an image in robot operational force space of the unit sphere defined in the actuated joint torque space:

$$\left\|\tilde{\boldsymbol{\tau}}\right\|^2 = \tilde{\boldsymbol{\tau}}^T \tilde{\boldsymbol{\tau}} = \tilde{\tau}_1^{\,2} + \tilde{\tau}_2^{\,2} + \cdots + \tilde{\tau}_l^{\,2} \le 1 \,. \tag{7}$$

It is described as

$$\boldsymbol{F}^T \boldsymbol{J}\boldsymbol{J}^T \boldsymbol{F} \le 1 \tag{8}$$

(Yoshikawa, 1990). However, in order to apply this method to evaluate the manipulability of the human upper limb, one must consider the differences of human joint torque characteristics on the joint rotational directions as defined in Eqs. (4) and (5). A simple way to do this evaluation is to map a unit sphere whose origin is the center position of joint torque described in Eq. (6) (Sasaki et al., 2004).

The center position of the set of all possible joint torque vectors can be written as

$$\tilde{\boldsymbol{\tau}}_{mean} = [\tilde{\tau}_{1mean}, \tilde{\tau}_{2mean}, \cdots, \tilde{\tau}_{lmean}]^T , \tag{9}$$

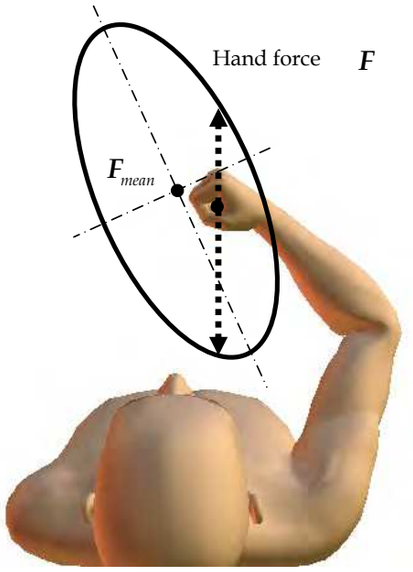

Fig. 2. Manipulating force ellipsoid based on human joint torque characteristics.

where

$$\tilde{\tau}_{imean} = \frac{\tilde{\tau}_{imax} + \tilde{\tau}_{imin}}{2} . \tag{10}$$

By assuming that $\tilde{\boldsymbol{\tau}}_{mean}$ is equal to the joint torque necessary to generate the hand force

$$\boldsymbol{F}_{mean} = [f_{1mean}, f_{2mean}, \cdots, f_{nmean}]^T , \tag{11}$$

the relation between $\tilde{\boldsymbol{\tau}}_{mean}$ and $\boldsymbol{F}_{mean}$ is given as

$$\tilde{\boldsymbol{\tau}}_{mean} = \boldsymbol{J}^T \boldsymbol{F}_{mean} , \tag{12}$$

where

$$f_{jmean} = \frac{f_{jmax} + f_{jmin}}{2} , \; j = 1, 2, \cdots, n . \tag{13}$$

Therein, f_{jmax} and f_{jmin} respectively signify the maximum hand force in the positive and negative directions.

The joint torque space, with origin $\tilde{\boldsymbol{\tau}}_{mean}$ is given by:

$$\tilde{\boldsymbol{\tau}} - \tilde{\boldsymbol{\tau}}_{mean} = \boldsymbol{J}^T (\boldsymbol{F} - \boldsymbol{F}_{mean}) . \tag{14}$$

By scaling Eq. (14) with the diagonal matrix we have:

$$\boldsymbol{T}_\tau = \mathrm{diag}\left(\frac{1}{\tilde{\tau}_{1max} - \tilde{\tau}_{1mean}}, \frac{1}{\tilde{\tau}_{2max} - \tilde{\tau}_{2mean}}, \cdots, \frac{1}{\tilde{\tau}_{lmax} - \tilde{\tau}_{lmean}} \right) , \tag{15}$$

the normalized joint torque is given as

$$\hat{\boldsymbol{\tau}} = \hat{\boldsymbol{J}}^T (\boldsymbol{F} - \boldsymbol{F}_{mean}) , \tag{16}$$

where,

$$\hat{\boldsymbol{\tau}} = \boldsymbol{T}_\tau (\tilde{\boldsymbol{\tau}} - \tilde{\boldsymbol{\tau}}_{mean}) \tag{17}$$

$$\hat{\boldsymbol{J}} = \boldsymbol{J}\boldsymbol{T}_{\tau}\,. \tag{18}$$

Therefore, the manipulating force ellipsoid, which reflects human joint torque characteristics maps the image in hand force spaces of a unit sphere in normalized joint torque space.

$$\|\hat{\boldsymbol{\tau}}\|^2 = \hat{\boldsymbol{\tau}}^T\hat{\boldsymbol{\tau}} = \hat{\tau}_1{}^2 + \hat{\tau}_2{}^2 + \cdots + \hat{\tau}_l{}^2 \le 1\,; \tag{19}$$

It is described as an *n*-dimensional hyperellipsoid

$$(\boldsymbol{F} - \boldsymbol{F}_{mean})^T\hat{\boldsymbol{J}}\hat{\boldsymbol{J}}^T(\boldsymbol{F} - \boldsymbol{F}_{mean}) \le 1\,. \tag{20}$$

Figure 2 portrays the proposed ellipsoid; the distance between the hand position and the ellipsoid surface shows the ease of hand force manipulation. Additionally, the difference between the push force and the pull force that can be added to the object is expressed quantitatively by defining the center of the ellipsoid as $\boldsymbol{F}_{mean}$. $\boldsymbol{F}_{mean}$ can be obtained directly from the relation between $\tilde{\boldsymbol{\tau}}_{mean}$ and $\boldsymbol{F}_{mean}$ defined by Eq. (12) when $\boldsymbol{J}$ is a regular matrix $(l = n)$. However, the device which replaces $\boldsymbol{F}_{mean}$ with the center position of the manipulating force polytope introduced in section 4 is needed because $\boldsymbol{F}_{mean}$, which balances $\tilde{\boldsymbol{\tau}}_{mean}$, does not necessarily exist when $\boldsymbol{J}$ is not a regular matrix $(l \ne n)$.

3.2 Visualization Algorithm for Higher Dimensional Hyperellipsoid

Visualization of the ellipsoid in four or more dimensions is extremely difficult. We propose a visualization algorithm for an *n*-dimensional hyperellipsoid using two projection methods: orthogonal projection and section. The difference between the orthogonal projection and section is whether to consider the influences of all components of the hand force vector to visualize the *n*-dimensional hyperellipsoid (see Fig. 3).

First, we describe the orthogonal projection. The influences of all components of the hand force vector are included in the *m*-dimensional ellipsoid $(m \le n)$ visualized by the orthogonal projection of the *n*-dimensional hyperellipsoid.

The *m*-component of the hand force vector that we visualize can be set arbitrarily as $\boldsymbol{F}_1$:

$$\boldsymbol{F} - \boldsymbol{F}_{mean} = [\boldsymbol{F}_1 \mid \boldsymbol{F}_2]^T = [\overline{f}_1, \cdots, \overline{f}_m \mid \overline{f}_{m+1}, \cdots, \overline{f}_n]^T\,, \tag{21}$$

where,

$$\overline{f}_j = f_j - f_{jmean}\,. \tag{22}$$

To satisfy the relation of Eq. (20), each component of $\hat{\boldsymbol{J}}\hat{\boldsymbol{J}}^T$ is according to the definition of Eq. (21).

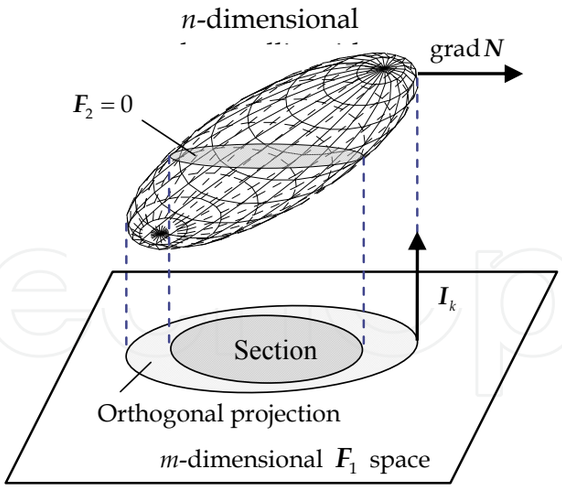

Fig. 3. Orthogonal projection and section of n-dimensional hyperellipsoid.

$$\hat{\boldsymbol{J}}\hat{\boldsymbol{J}}^T = \left[\begin{array}{ccc|cc} h_{1,1} & h_{1,2} & \cdots & \cdots & h_{1,n} \\ h_{2,1} & \ddots & & & \vdots \\ \vdots & & h_{m,m} & & \vdots \\ \hline \vdots & & & \ddots & \vdots \\ h_{n,1} & \cdots & \cdots & \cdots & h_{n,n} \end{array}\right] = \left[\begin{array}{c|c} \boldsymbol{A} & \boldsymbol{B} \\ \hline \boldsymbol{C} & \boldsymbol{D} \end{array}\right], \tag{23}$$

where $\boldsymbol{A} \in \boldsymbol{R}^{m\times m}$, $\boldsymbol{B} \in \boldsymbol{R}^{m\times(n-m)}$, $\boldsymbol{C} \in \boldsymbol{R}^{(n-m)\times m}$ and $\boldsymbol{D} \in \boldsymbol{R}^{(n-m)\times(n-m)}$ are submatrices of real symmetric matrix $\hat{\boldsymbol{J}}\hat{\boldsymbol{J}}^T \in \boldsymbol{R}^{n\times n}$.

The vertical vector to the n-dimensional hyperellipsoid is equal to the gradient vector

$$\operatorname{grad}\boldsymbol{N} = \left[\frac{\partial \boldsymbol{N}}{\partial \bar{f}_1}, \frac{\partial \boldsymbol{N}}{\partial \bar{f}_2}, \cdots, \frac{\partial \boldsymbol{N}}{\partial \bar{f}_n}\right]^T, \tag{24}$$

where

$$\boldsymbol{N} = (\boldsymbol{F} - \boldsymbol{F}_{mean})^T \hat{\boldsymbol{J}}\hat{\boldsymbol{J}}^T (\boldsymbol{F} - \boldsymbol{F}_{mean}) - 1 . \tag{25}$$

The $(n-m)$ vertical unit vectors to the m-dimensional $\boldsymbol{F}_1$ space are given as shown below.

$$\begin{aligned} \boldsymbol{I}_1 &= [0,\cdots,0,1,0,\cdots,0]^T \\ &\vdots \\ \boldsymbol{I}_{n-m} &= [\underbrace{0,\cdots,0}_{m},\underbrace{0,0,\cdots,1}_{n-m}]^T \end{aligned} \tag{26}$$

To express the orthogonal projection of the n-dimensional hyperellipsoid to the m dimensional $\boldsymbol{F}_1$ space, the unit vector $\boldsymbol{I}_k$ $(k = 1,2,\cdots,n-m)$ must be an orthogonal relation to the vertical vector $\operatorname{grad}\boldsymbol{N}$, as depicted in Fig. 3

$$\operatorname{grad}\boldsymbol{N} \bullet \boldsymbol{I}_k = 0 . \tag{27}$$

Substituting Eqs. (24) and (26) into Eq. (27), we obtain

$$\begin{aligned}\frac{\partial \boldsymbol{N}}{\partial \overline{f}_{m+1}} &= h_{m+1,1}\overline{f}_1 + h_{m+1,2}\overline{f}_2 + \cdots + h_{m+1,n}\overline{f}_n = 0 \\ &\vdots \\ \frac{\partial \boldsymbol{N}}{\partial \overline{f}_n} &= h_{n,1}\overline{f}_1 + h_{n,2}\overline{f}_2 + \cdots + h_{n,n}\overline{f}_n = 0\end{aligned} \quad . \tag{28}$$

Equation (28) expresses the orthogonal condition for the orthogonal projection. Using the definition described in Eqs. (21) and (23), the orthogonal condition can be written as

$$\boldsymbol{C}\boldsymbol{F}_1 + \boldsymbol{D}\boldsymbol{F}_2 = 0 \tag{29}$$

$$\boldsymbol{F}_2 = -\boldsymbol{D}^{-1}\boldsymbol{C}\boldsymbol{F}_1 \,. \tag{30}$$

Therefore, the general equations of the orthogonal projection are given as

$$(\boldsymbol{F} - \boldsymbol{F}_{mean})^T \hat{\boldsymbol{J}}\hat{\boldsymbol{J}}^T (\boldsymbol{F} - \boldsymbol{F}_{mean}) = [\boldsymbol{F}_1 \;\; \boldsymbol{F}_2]\begin{bmatrix}\boldsymbol{A} & \boldsymbol{B} \\ \boldsymbol{C} & \boldsymbol{D}\end{bmatrix}\begin{bmatrix}\boldsymbol{F}_1 \\ \boldsymbol{F}_2\end{bmatrix} = \boldsymbol{F}_1^T (\boldsymbol{A} - \boldsymbol{B}\boldsymbol{D}^{-1}\boldsymbol{C})\boldsymbol{F}_1 \,. \tag{31}$$

Additionally, using the orthogonal transformation from $\boldsymbol{F}_1$ space to $\boldsymbol{E}$ space

$$\boldsymbol{F}_1 = \boldsymbol{P}\boldsymbol{E} \tag{32}$$

$$\boldsymbol{E} = [e_1, e_2, \cdots, e_m]^T \,, \tag{33}$$

Eq. (31) can be written in the following normal form

$$\boldsymbol{F}_1^T (\boldsymbol{A} - \boldsymbol{B}\boldsymbol{D}^{-1}\boldsymbol{C})\boldsymbol{F}_1 = \boldsymbol{E}^T \boldsymbol{P}^T (\boldsymbol{A} - \boldsymbol{B}\boldsymbol{D}^{-1}\boldsymbol{C})\boldsymbol{P}\boldsymbol{E} = \lambda_1 e_1^{\,2} + \lambda_2 e_2^{\,2} + \cdots + \lambda_m e_m^{\,2} = 1 \,, \tag{34}$$

where λ_r $(r = 1, 2, \cdots, m)$ are eigenvalues of $(\boldsymbol{A} - \boldsymbol{B}\boldsymbol{D}^{-1}\boldsymbol{C})$, $\boldsymbol{P} \in \boldsymbol{R}^{m \times m}$ signifies the orthogonal matrix whose columns are the eigenvectors $\boldsymbol{p}_r$ of $(\boldsymbol{A} - \boldsymbol{B}\boldsymbol{D}^{-1}\boldsymbol{C})$, the principal axes and directions of the *m*-dimensional ellipsoid are denoted, respectively, as $1/\sqrt{\lambda_r}$ and $\boldsymbol{p}_r$.

Next, we explain another visualization algorithm viz. section. The *m*-dimensional ellipsoid visualized by the section of the *n*-dimensional hyperellipsoid shows the set of generatable hand force vectors under $\boldsymbol{F}_2 = 0$ (see Fig. 3). Therefore, by substituting $\boldsymbol{F}_2 = 0$ into Eq. (31), the general equations of sectioning are given as

$$(\boldsymbol{F} - \boldsymbol{F}_{mean})^T \hat{\boldsymbol{J}}\hat{\boldsymbol{J}}^T (\boldsymbol{F} - \boldsymbol{F}_{mean}) = [\boldsymbol{F}_1 \;\; 0]\begin{bmatrix}\boldsymbol{A} & \boldsymbol{B} \\ \boldsymbol{C} & \boldsymbol{D}\end{bmatrix}\begin{bmatrix}\boldsymbol{F}_1 \\ 0\end{bmatrix} = \boldsymbol{F}_1^T \boldsymbol{A}\boldsymbol{F}_1 \,. \tag{35}$$

Using the orthogonal transformation from $\boldsymbol{F}_1$ space to $\boldsymbol{W}$ space

$$\boldsymbol{F}_1 = \boldsymbol{Q}\boldsymbol{W} \tag{36}$$

$$\boldsymbol{W} = [w_1, w_2, \cdots, w_m]^T \,, \tag{37}$$

Eq. (35) can also be written as

$$\boldsymbol{F}_1^T \boldsymbol{A}\boldsymbol{F}_1 = \boldsymbol{W}^T \boldsymbol{Q}^T \boldsymbol{A}\boldsymbol{Q}\boldsymbol{W} = \mu_1 w_1^{\,2} + \mu_2 w_2^{\,2} + \cdots + \mu_m w_m^{\,2} = 1 \,, \tag{38}$$

where μ_r $(r = 1, 2, \cdots, m)$ are eigenvalues of $\boldsymbol{A}$, $\boldsymbol{Q} \in \boldsymbol{R}^{m \times m}$ signifies the orthogonal matrix whose columns are the eigenvectors $\boldsymbol{q}_r$ of $\boldsymbol{A}$, the principal axes and directions of the *m* dimensional ellipsoid are given, respectively, by $1/\sqrt{\mu_r}$ and $\boldsymbol{q}_r$.

Equations (34) and (38) show that an *n*-dimensional hyperellipsoid that cannot be viewed directly is expressible as a visible *m*-dimensional ellipsoid using orthogonal projection or sectioning. The proposed visualization algorithm is applicable to evaluation of the hand force characteristics suitable for the purpose because hand force $\boldsymbol{F}_1$ in Eq. (21) can be defined freely.

3.3 Experimental Validation

The proposed evaluation method is verified by comparing the manipulating force ellipsoid based on maximum joint torque with the measured hand force characteristics.

3.3.1 Measurement of Maximum Joint Torque

In order to calculate the manipulating force ellipsoid reflecting an individual's joint torque characteristics, it is indispensable to measure the maximum joint torque $\tau_{imax}(\theta_i)$ and $\tau_{imin}(\theta_i)$ in advance. For these studies, a Cybex machine (Cybex Inc.) was used for measuring them. The device can measure the maximum joint torque continuously at every joint angle in both the positive and negative directions.

For our experiment, we measured the maximum joint torque produced by the concentric contraction for every pair of movement directions; flexion and extension, adduction and abduction, and external rotation and internal rotation at the shoulder; flexion and extension at the elbow; and supination and pronation, palmar flexion and dorsiflexion, and radial flexion and ulnar flexion at the wrist (see Fig. 4). The subject in the experiment was a healthy young person (21 years old, 180 cm, and 60 kg). The purpose of this research was explained to the subject before the experiment.

3.3.2 Measurement of the Hand Force and Joint Angle

(a) Shoulder flexion/extension

(b) Shoulder adduction/abduction

(c) Shoulder external/internal rotation

(d) Elbow flexion/extension

(e) Wrist supination/pronation

(f) Wrist palmar flexion/dorsiflexion

(g) Wrist radial flexion/ulnar flexion

Fig. 4. Measurement of maximum joint torque.

Figure 5 shows a measurement system comprising a six-axis force sensor (IFS-105M50A20-I63; Nitta Corp.) and a three-dimensional magnetic position and orientation sensor (Fastrak;Polhemus). The subject added the hand force in eight directions using maximum effort. The hand force applied to a grip was measured using the six-axis force sensor. The receiver to detect the position and posture was put to the hand and the humerus. The joint position and angle of the upper limb, which has 7 degrees of freedom, was calculated using the method developed by Oikawa and Fujita (2000). During this measurement, the subject's upper body was fixed to the back of a chair by belts to eliminate the influence of upper body movements on maximum hand force measurements. The measurements were taken at a sampling frequency of 20 Hz.

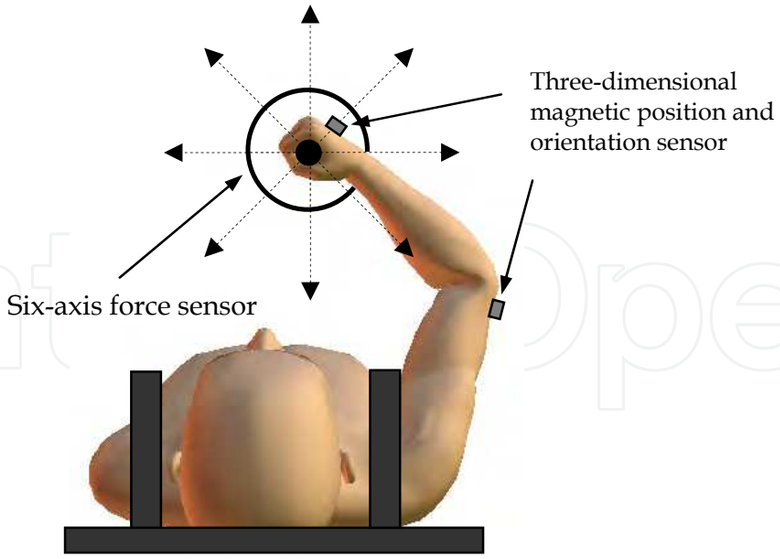

Fig. 5. Measurement system for hand force and upper limb posture.

3.3.3 Results

Figure 6 depicts a typical example of the maximum joint torque measured using the Cybex device. It is very clear that the ellipsoid described above, which does not consider human joint torque characteristics, is insufficient to evaluate the manipulability of upper limbs because even the joint torque characteristics of healthy person vary greatly according to the joint angle and rotational direction.

Figure 7 portrays a two-dimensional ellipsoid calculated from the maximum joint torque and the posture of the upper limb under the definition of

$$\boldsymbol{F} - \boldsymbol{F}_{mean} = [\boldsymbol{F}_1 \mid \boldsymbol{F}_2]^T = [f_x, f_y \mid f_z, m_x, m_y, m_z]^T , \tag{39}$$

where f , m , and subscripts signify the hand force, moment, and its direction respectively. A large ellipse represents the orthogonal projection of the six-dimensional hyperellipsoid and shows the set of all hand force vectors that can be generated under constraint conditions defined in Eq. (19). A small ellipse represents the section of the six-dimensional hyperellipsoid and means the set of generatable hand force vector under $\boldsymbol{F}_2 = 0$. On the other hand, circles in Fig. 7 show the measured hand force. Furthermore, the hand force is represented as a black circle when the joint torque to generate the measured hand force is satisfied as per the constraint condition of Eq. (19). A distribution map of the circle shows

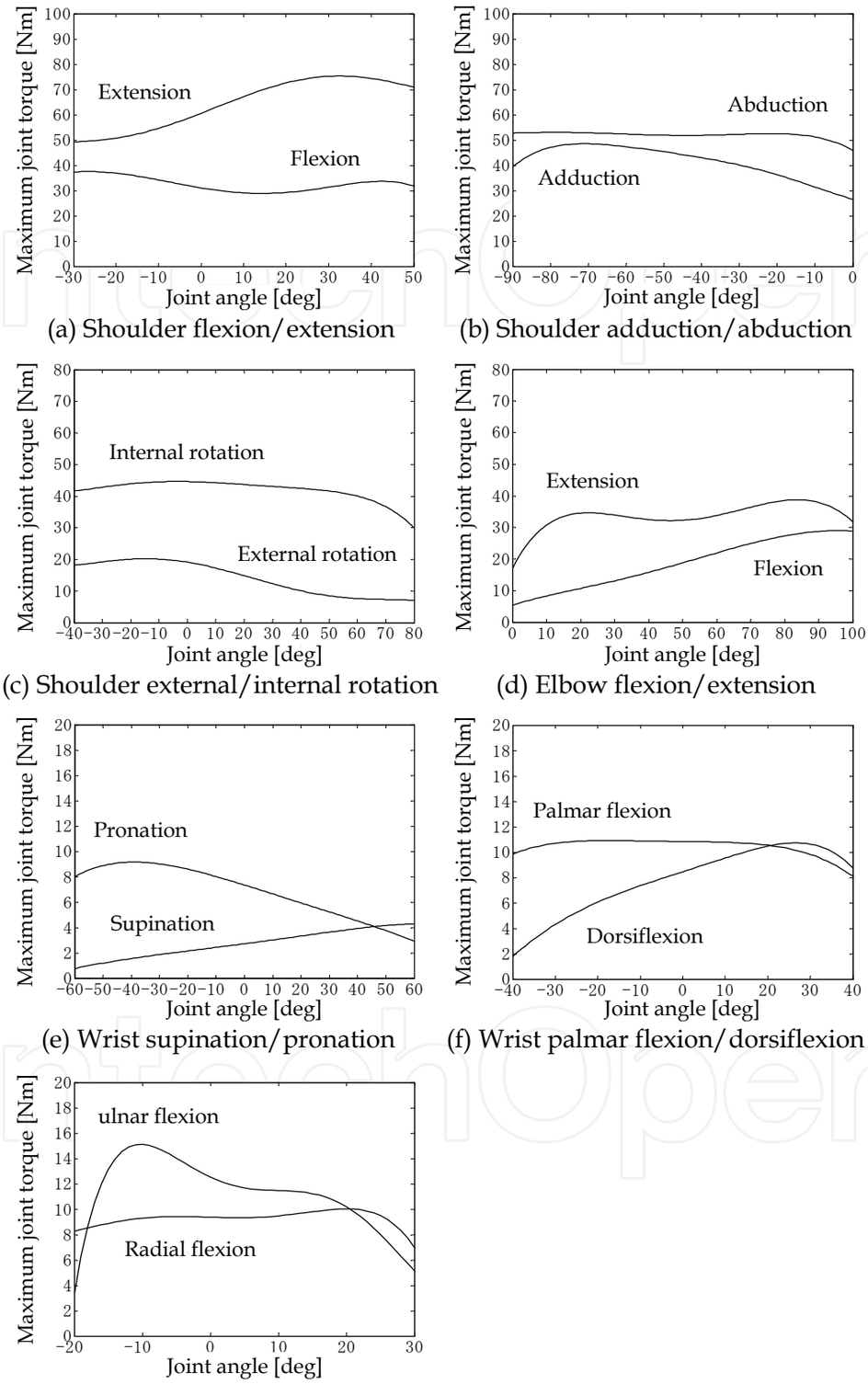

(a) Shoulder flexion/extension (b) Shoulder adduction/abduction

(c) Shoulder external/internal rotation (d) Elbow flexion/extension

(e) Wrist supination/pronation (f) Wrist palmar flexion/dorsiflexion

(g) Wrist radial flexion/ulnar flexion

Fig. 6. Measurement results of maximum joint torque.

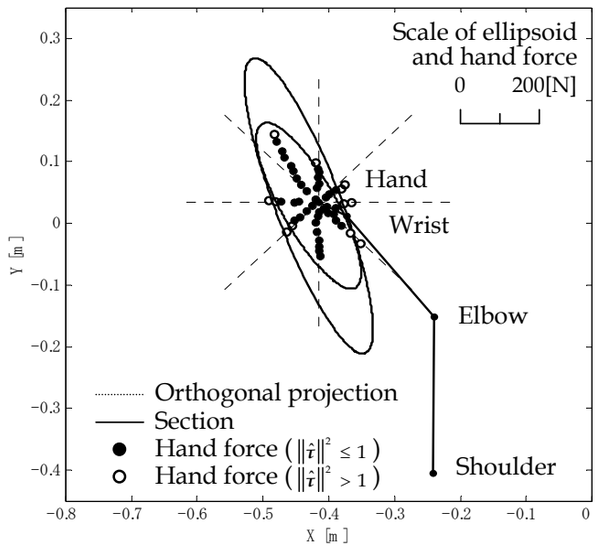

Fig. 7. Manipulating force ellipsoid and hand force.

that the magnitude of the push force and pull force in a certain direction is different. Also the ellipse visualized by the section is suitable for expression of the subject's manipulability of the upper limb in this experimental condition because the small ellipse and the black circle almost correspond to each other. One reason is that the influence of force $\boldsymbol{F}_2$ on the measured force appears only slightly because we instructed the subject to apply hand force simply on the horizontal plane.

The effectiveness of the new method proposed for quantitative evaluation of the individual's manipulability of the upper limb can be verified through the experimental results.

4. Manipulating Force Polytope Considering Joint Torque Characteristics

The manipulating force ellipsoid based on human joint torque characteristics represents the set of generatable hand force in the constraint condition of Eq. (19). It is effective for evaluation of the ease of hand force manipulation. However, to develop an assistive device that makes the best use of the remaining function, it is also important to evaluate the set of hand forces that can be generated using all joint torques defined in Eq. (6). We introduce the manipulating force polytope based on human joint torque characteristics, along with its vertex search algorithm (Sasaki et al., 2007a).

4.1 Derivation of the Polytope

All the hand forces that can be generated in a daily life motion is given by the joint torques satisfying the condition of Eq. (6). The set of all hand forces can be calculated using Eq. (6) and

$$\boldsymbol{F} = (\boldsymbol{J}^T)^{-1}\tilde{\boldsymbol{\tau}} . \tag{40}$$

This set of forces can be expressed as a convex polytope in n-dimensional hand force space.

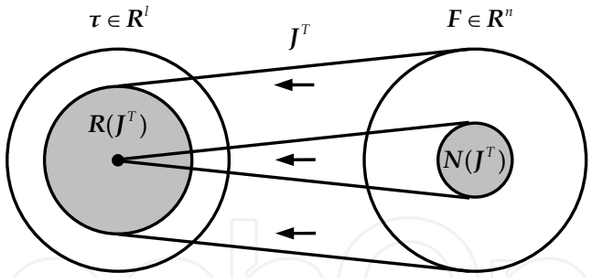

Fig. 8. Null space and range space of J^T.

The convex polytope can be called a manipulating force polytope. For a redundant manipulator such as the human upper limb $(l > n)$, in general, the set of hand forces cannot be calculated directly because J^T is not a regular matrix. The pseudo-inverse matrix $(J^T)^+$ is a general solution that minimizes the error norm $\left\|\tilde{\tau} - J^T F\right\|$ and it is introduced instead of $(J^T)^{-1}$

$$F = (J^T)^+ \tilde{\tau}\,, \tag{41}$$

(Chiacchio et al., 1997). However, Eq. (3) does not always have a solution for hand force because all joint torque space cannot be covered with the range space $R(J^T)$ of J^T, as shown in Fig. (8) (Asada & Slotine, 1986). In other words, a unique solution is not guaranteed and $\tilde{\tau}$ of both sides of the following equation is not always corresponding.

$$\tilde{\tau} = J^T F = J^T (J^T)^+ \tilde{\tau} = \tilde{\tau} \tag{42}$$

Therefore, to obtain the manipulating force polytope for a human upper limb, searching the subspace of the joint torque space given by $R(J^T)$ and projecting it to the hand force space are required.

Here, because the null space $N(J)$ of J is an orthogonal complement of $R(J^T)$, the following relation can be written

$$N(J) = \{R(J^T)\}^{\perp}\,. \tag{43}$$

In addition, the singular value decomposition of Jacobian matrix J is given as

$$J = U\Sigma V^T = [U_1 \;\; U_2]\begin{bmatrix} S & 0 \\ 0 & 0 \end{bmatrix}\begin{bmatrix} V_1^T \\ V_2^T \end{bmatrix}, \tag{44}$$

where $\Sigma \in R^{n\times l}$ is a diagonal matrix with arranged nonzero singular values of J such as $S = \mathrm{diag}(s_1, s_2, \cdots, s_r)$, $U \in R^{n\times n}$ is an orthogonal matrix, $U_1 \in R^{n\times r}$ and $U_2 \in R^{n\times(n-r)}$ are submatrices of U, $V \in R^{l\times l}$ is an orthogonal matrix, $V_1 \in R^{l\times r}$ and $V_2 \in R^{l\times(l-r)}$ are submatrices of V, and r is the rank of J. Because the column vector v_t $(t = 1,2,\cdots,r)$ of V_1 is equal to the base vector of Eq. (43), $R(J^T)$ is represented as the space covered by r base vectors of dimension l. By projecting to the hand force space the joint torque's subspace given by $R(J^T)$, the manipulating force polytope is obtainable.

4.2 Vertex Search Algorithm for Higher Dimensional Polytope

To search for the vertex of the convex polytope, a slack variable is generally introduced. However, the vertex search using a linear programming method such as the simplex

method engenders huge computational complexity and a complex definition of the objective function. Especially, it is extremely difficult to search for all vertexes of a high-dimensional polytope. Therefore, we propose a new vertex search algorithm.

The vertex search algorithm is based on the geometric characteristic that the points of intersection between the *l*-dimensional joint torque space and the space covered by r base vectors of dimension l exist in the $(l-r)$ -dimensional face of joint torque space. The algorithm is explained using a three-dimensional rectangle in Fig. 9 for clarification.

For $l=3$ and $r=2$, the two-dimensional plane covered by two base vectors intersects with a side (= one dimension) of a three-dimensional rectangle (see Fig. 9(a)). Because its side is a common set of two planes, the number of joint torque components equal to the maximum joint torque $\tilde{\tau}_{imax}$ or the minimum joint torque $\tilde{\tau}_{imin}$ is equal to two. For $l=3$ and $r=1$, the one-dimensional straight line covered by a base vector intersects with a face (= two dimension) of a three-dimensional rectangle (see Fig. 9(b)). The number of joint torque components equal to $\tilde{\tau}_{imax}$ or $\tilde{\tau}_{imin}$ is then equal to one. Consequently, generalizing the geometric characteristics shows that the space covered by r base vectors of dimension l intersects with the $(l-r)$ -dimensional face of the *l*-dimensional joint torque space. It also reveals that the number of joint torque components equal to $\tilde{\tau}_{imax}$ or $\tilde{\tau}_{imin}$ is equal to r.

By defining the points of intersection between the *l*-dimensional joint torque space and the range space $\boldsymbol{R}(\boldsymbol{J}^T)$ of $\boldsymbol{J}^T$ as

$$\boldsymbol{K}=[k_1,k_2,\cdots,k_r]^T, \tag{45}$$

the subspace of the joint torque space is given as

$$\boldsymbol{T}=k_1\boldsymbol{v}_1+k_2\boldsymbol{v}_2+\cdots+k_r\boldsymbol{v}_r=\boldsymbol{V}_1\boldsymbol{K}. \tag{46}$$

Equation (46) can also be written as

$$\begin{bmatrix}\boldsymbol{T}_1\\ \boldsymbol{T}_2\end{bmatrix}=\begin{bmatrix}\tau_1\\ \vdots\\ \tau_r\\ \tau_{r+1}\\ \vdots\\ \tau_l\end{bmatrix}=\begin{bmatrix}k_1v_{11}+k_2v_{21}+\cdots+k_rv_{r,1}\\ \vdots\\ k_1v_{1,r}+k_2v_{2,\mathrm{r}}+\cdots+k_rv_{r,r}\\ k_1v_{1,r+1}+k_2v_{2,r+1}+\cdots+k_rv_{r,r+1}\\ \vdots\\ k_1v_{1,l}+k_2v_{2,l}+\cdots+k_rv_{r,l}\end{bmatrix}=\begin{bmatrix}\boldsymbol{V}_{11}\\ \boldsymbol{V}_{12}\end{bmatrix}\boldsymbol{K}, \tag{47}$$

where $\boldsymbol{T}_1\in\boldsymbol{R}^r$ and $\boldsymbol{T}_2\in\boldsymbol{R}^{l-r}$ are submatrices of $\boldsymbol{T}\in\boldsymbol{R}^l$, and where $\boldsymbol{V}_{11}\in\boldsymbol{R}^{r\times r}$ and $\boldsymbol{V}_{12}\in\boldsymbol{R}^{(l-r)\times r}$ are the submatrices of the base vector $\boldsymbol{V}_1$. From this equation, the relation between $\boldsymbol{T}_1$ and $\boldsymbol{T}_2$ is obtained as

$$\boldsymbol{T}_2=\boldsymbol{V}_{12}\boldsymbol{K}=\boldsymbol{V}_{12}\boldsymbol{V}_{11}{}^{-1}\boldsymbol{T}_1. \tag{48}$$

Because there are ' r ' joint torque components equal to $\tilde{\tau}_{imax}$ or $\tilde{\tau}_{imin}$ in the intersection points, we can define $\boldsymbol{T}_1$ as shown below:

$$\boldsymbol{T}_{11}=\begin{bmatrix}\tau_1\\ \vdots\\ \tau_r\end{bmatrix}=\begin{bmatrix}\tilde{\tau}_{1max}\ \ or\ \ \tilde{\tau}_{1min}\\ \vdots\\ \tilde{\tau}_{rmax}\ \ or\ \ \tilde{\tau}_{rmin}\end{bmatrix} \tag{49}$$

The points of intersection $\boldsymbol{K}$ are obtained by judging whether the joint torque component of $\boldsymbol{T}_2$ calculated from Eqs. (48) and (49) satisfies the condition of the joint torque in Eq. (6). Therefore only when $\boldsymbol{T}_2$ satisfies this condition, the joint torque $\boldsymbol{T}$ is calculated from $\boldsymbol{K}$,

$$\boldsymbol{K} = \boldsymbol{V}_{11}{}^{-1}\boldsymbol{T}_1 = \boldsymbol{V}_{12}{}^{-1}\boldsymbol{T}_2 , \tag{50}$$

And it becomes the vertex of the *l*-dimensional convex polytope. Herein, the number of combinations which select the *n* equations from *l* equations in Eq. (47) and define $\boldsymbol{V}_{11}$ is ${}_lC_r$, while the number of combinations defining $\boldsymbol{T}_1$ in Eq. (49) is 2^r. All vertexes of the *l* dimensional convex polytope can be found by calculating the intersection points in all combinations. The manipulating force polytope based on human joint torque characteristics is finally expressed by calculating the convex hulls of all the vertexes projected using Eq. (41) on the hand force space. This is done because the vertex of the *l*-dimensional convex polytope defined by the proposed algorithm always guarantees the unique solution shown in Eq. (42).

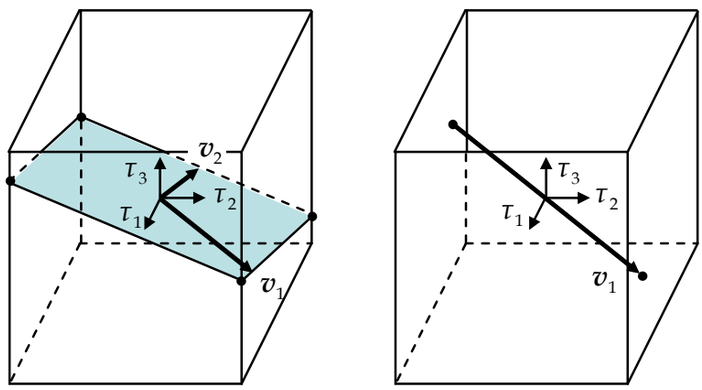

(a) $l = 3$, $r = 2$ (b) $l = 3$, $r = 1$

Fig. 9. Vertexes of *l*-dimensional convex polytopes.

4.3 Experimental Validation

To evaluate the effectiveness of the proposed method, an experiment to compare the manipulating force polytope based on maximum joint torque with the measured hand force characteristics was performed. The experimental methodology and the device were identical to those shown in subsection 3.3. The participant in the experiment was a person with a spinal cord injury (60 years old, 170 cm, 55 kg, and L2 lumbar injury).

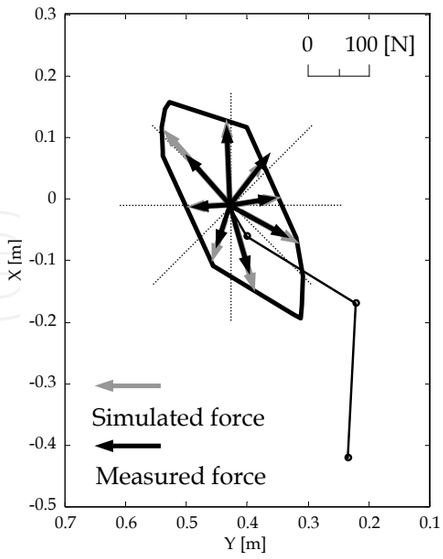

Fig. 10. Manipulating force polytope and hand force.

Figure 10 portrays the manipulating force polytope, as calculated from the maximum joint torque and posture of the upper limb. The polytope, projected to the two-dimensional plane, represents the set of all the possible hand force on the horizontal plane, demonstrating a hexagonal shape. This feature of shape of the manipulating force polytope agrees with findings of Oshima et al. (1999) that the distribution of the hand force vector in a two-dimensional plane is a hexagonal shape. In addition, the hand force vector (gray arrow) presumed from the manipulating force polytope approximately corresponds to the measured hand force (black arrow). The effectiveness of the method proposed for quantitative evaluation of the individual's manipulability of the upper limb can be confirmed through the presented experimental result, but it is necessary to perform further verification to achieve a more accurate evaluation.

5. Application to Wheelchair Propulsion

The proposed evaluation methods are useful for developing assistive devices, planning of rehabilitation, and improving living environments because an individual's manipulability of the upper limb can be evaluated quantitatively and visually. As a practical application of the proposed methods, we present the analysis of wheelchair propulsion.

Wheelchairs are commonly used mobility devices that support people for whom walking is difficult or impossible because of illness, injury, or disability. However, more than 50% of all manual wheelchair users experience upper limb pain or injury (Gellman et al., 1988; Sie et al., 1992; Pentland & Twomey, 1994). The most common problems of wheelchair users, who push on the handrim an average of 2000–3000 times a day, are shoulder, wrist, and hand injuries including carpal tunnel syndrome. For these reasons, studies of wheelchair propulsion have mainly addressed the physical load borne by wheelchair users, in addition to technical improvements, wheelchair configurations, and design optimization (Cooper,

1998; Engstrom, 2002; Sasaki et al., 2007b, 2008). A study related to optimal wheelchair design that we performed, (analytical results of wheelchair propulsion using the manipulating force ellipsoid) based on human joint torque characteristics is described here.

5.1 Experiments

The participants in the experiment were eight experienced wheelchair users with spinal cord injuries (55±15 years old, 167.5±7.5 cm, 63.5±11.5 kg, and injury levels T12–L2). In the experiment the maximum joint torque characteristics of the upper limb were measured using the Cybex machine portrayed in Fig. 4. The upper limb movement and hand force during wheelchair propulsion were measured using the measurement system presented in Fig. 11. The system comprises a three-dimensional magnetic position and orientation sensor (Fastrak; Polhemus) for measuring the joint angle and joint position of the upper limb. A six-axis force sensor (IFS-67M25A-I40; Nitta Corp.) for measuring the three-directional force and moment applied to the handrim, and a rotary encoder (OHI48-6000P4-L6-5V; Tamagawa Seiki Co. Ltd.) for measuring the rear wheel's rotation angle. Based on advice from an occupational therapist, the height of the rear wheel axis was adjusted to become equal with the subject's hand position when the hand was hung straight downward.

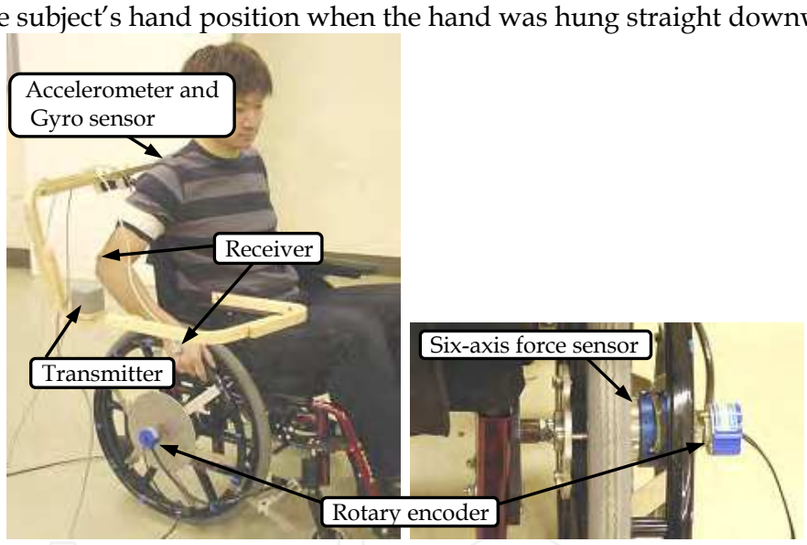

Fig. 11. Measurement system for hand force and upper limb posture during wheelchair propulsion.

5.2 Analysis of Wheelchair Maneuverability

Figure 12 portrays the measurement results of the upper limb postures and force vectors applied to the handrim, in addition to the calculation results of the manipulating force ellipsoid based on maximum joint torque characteristics as the stick diagram on the (a) sagittal plane and (b) frontal plane. Because most wheelchair users do not grasp the handrim during wheelchair propulsion, the ellipsoid was projected to each plane under the condition that all moment components are zero. In general, an increase of the hand force component toward the handrim tangential direction is necessary to achieve efficient wheelchair propulsion, because the handrim has only one degree of freedom which is rotation around the rear wheel axis. To analyze the wheelchair maneuverability

quantitatively, the parameters presented in Fig. 13 were defined as $\boldsymbol{F}_m$ is the maximum generatable force, φ is the hand contact position, and a and β are angles on each plane between $\boldsymbol{F}_m$ and the most effective force direction d_{mef}.

Figures 14 and 15 respectively portray calculation results of the maximum generatable force $\boldsymbol{F}_m$, the angle a on the sagittal plane, and angle β on the frontal plane. The bands in the figure present the average value ± standard deviation among all subjects. Strong hand force is applicable to the handrim efficiently in the latter half of the propulsion cycle. This is because an increase in the maximum generatable force $\boldsymbol{F}_m$ and a decrease in angle a can be confirmed from the figure. However, angle a differs by more than 80 deg in the first half of the propulsion cycle. In this phase, the hand force applied in the direction $\boldsymbol{F}_m$ will not generate a sufficient hand force component in direction d_{mef}, which contributes directly to driving a wheelchair. Even if it is purely applied in the direction d_{mef}, the physical load of the upper limb will increase because d_{mef} is the direction in which wheelchair users have difficult applying hand force. Consequently, the fact that the users must start driving the wheelchair from an upper limb posture with bad maneuverability is inferred as one of the factors increasing the physical load of wheelchair users.

On the other hand, by looking at angle β on the frontal plain, it is very apparent that the direction to which the hand force can be generated easily, i.e., the direction of $\boldsymbol{F}_m$, differs from direction d_{mef} by about 5–10 deg. It shows that attaching the camber angle for the rear wheel is an efficient way to transmit hand force. The camber angle is known to be efficient for producing lateral stability of a wheelchair, reducing the downward turning tendency on side slopes, and preventing interference between the upper limb and the handrim (Trudel et al., 1995; Cooper, 1998). Furthermore, using the proposed evaluation methods, the effectiveness of the camber angle was proved from the new viewpoint of manipulability of the upper limb, bringing ease of hand force manipulation to wheelchair users.

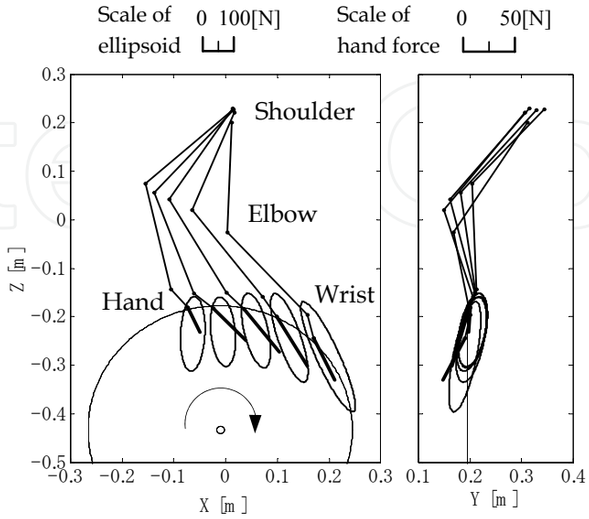

(a) Sagittal plane (b) Frontal plane

Fig. 12. Stick diagram of the upper limb, hand force, and manipulating force ellipsoid.

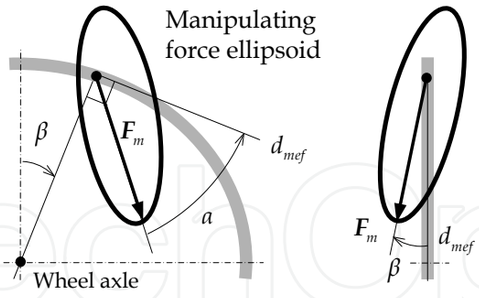

(a) Sagittal plane (b) Frontal plane

Fig. 13. Definition of component and angle of manipulating force ellipsoid.

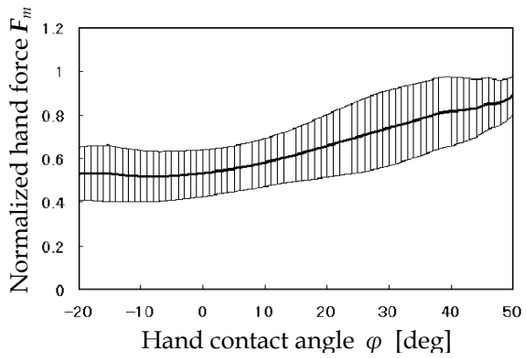

Fig. 14. Maximum generatable hand force F_m .

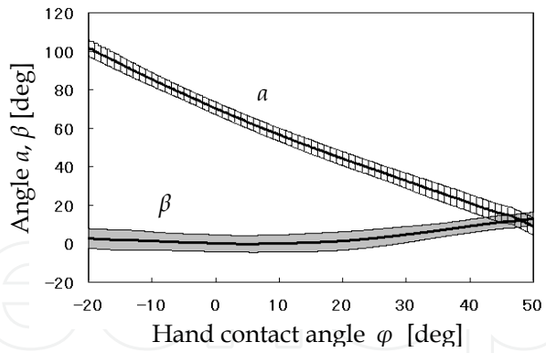

Fig. 15. Angle between maximum generatable hand force F_m and mechanically most effective force direction d_{mef} .

5.3 Analysis of Hand Force Patterns

Next, we analyze the hand force patterns applied to the handrim. The stick diagram of Fig. 12 shows that the direction of the measured hand force does not necessarily correspond to the direction in which the maximum hand force can be generated. One reason is that the hand force applied in direction of F_m does not necessarily engender an efficient driving force, as clearly depicted in the results portrayed in Fig. 15. However, it is readily inferred

that long-term wheelchair users perform efficient propulsion patterns. Therefore, we propose a new concept of the driving force contribution figure reflecting the driving efficiency to the manipulating force ellipsoid. Thereafter, we analyze hand force patterns used in wheelchair propulsion.

The driving force contribution figure is the set of driving forces obtainable using all hand force components of the manipulating force ellipsoid (see Fig. 16) and the driving force $\boldsymbol{F}_e$ is

$$\boldsymbol{F}_e = \frac{|\boldsymbol{F}_t|}{|\boldsymbol{F}_a|}\boldsymbol{F}_a , \tag{51}$$

where $\boldsymbol{F}_a$ is an arbitrary hand force vector in the manipulating force ellipsoid, and where $\boldsymbol{F}_t$ is a tangential component of $\boldsymbol{F}_a$ to the handrim, directly contributing to driving a wheelchair. In addition, driving force $\boldsymbol{F}_e$ has a direction equal to $\boldsymbol{F}_a$ and magnitude equal to $\boldsymbol{F}_t$. The distance between the boundary of the driving force contribution figure and the hand position on the handrim represents the contribution to driving the wheelchair. In other words, if the driving force contribution figure takes a large value along the driving force direction, the applied hand force efficiently supports wheelchair propulsion.

Figure 17 portrays a stick diagram, which is a product of the driving force contribution figure and Fig. 11. To analyze this numerical result more quantitatively, the parameters

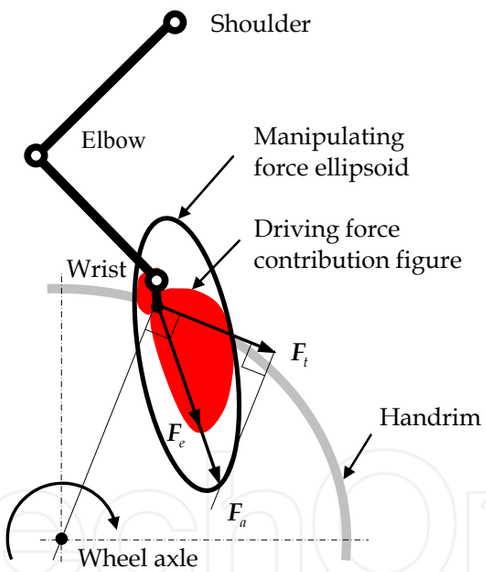

Fig. 16. Definition of driving force contribution figure.

presented in Fig. 18 were defined as follows: $\boldsymbol{F}_{em}$ signifies the maximum driving force, $\boldsymbol{F}_s$ denotes the hand force applied to the handrim, $\boldsymbol{F}_{ts}$ stands for a tangential component of $\boldsymbol{F}_s$ to the handrim, φ represents the hand contact position, and a' and β' are angles on each plane between $\boldsymbol{F}_{em}$ and the measured force $\boldsymbol{F}_s$.

Figures 19 and 20 respectively portray the calculation results of the maximum driving force $\boldsymbol{F}_{em}$, the tangential component of measured force $\boldsymbol{F}_{ts}$, the angle a' on the sagittal plane and

the angle β' on the frontal plane. The bands in the figure present average values ± standard deviation among all subjects, showing that possible hand forces expressed by the manipulating force ellipsoid can be converted efficiently into the driving force in the latter half of the propulsion cycle because the maximum generatable driving force $\boldsymbol{F}_{em}$ increases gradually. The results show that angle α' on the sagittal plain is about 10 degrees and angle β' on the frontal plain is 20 degrees, except for the time when the wheelchair starts to move. In addition, the force of the wheelchair users was applied to the direction in which the driving force can be generated easily. Based on the fact that most wheelchair users do not grasp the handrim during wheelchair propulsion, it can be understood that the hand force applied to the perpendicular direction to the handrim is also necessary to transmit the hand force to the tangential direction to the hand rim, although it does not contribute directly to driving. Especially at the time a wheelchair is moved from its halted state, the friction force between the hand and the handrim is required. That is thought to be the reason for the difference of the hand force direction, as presented in Fig. 20. Taken together, all these results reflect that the wheelchair users are considering both the efficiency and physical load of the upper limb, and are performing a very skillful operation for the task that they are given for wheelchair propulsion. This is confirmed to be true because, except for the time when a wheelchair must be moved initially, the direction in which the hand force is actually applied agrees mostly with the direction in which the driving force can be easily produced.

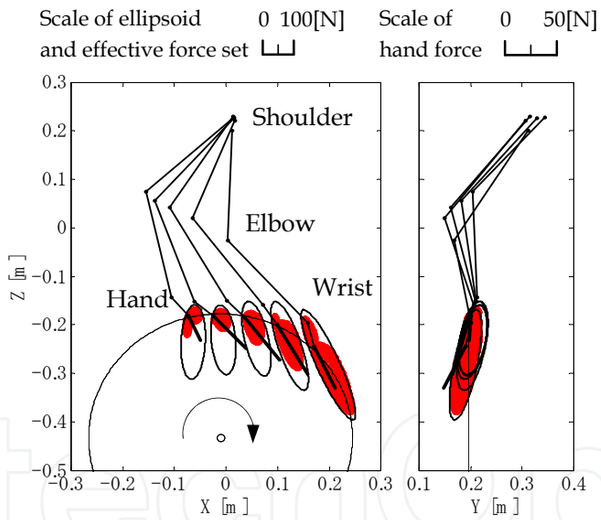

(a) Sagittal plane (b) Frontal plane

Fig. 17. Stick diagram of the upper limb, hand force, manipulating force ellipsoid, and driving force contribution figure.

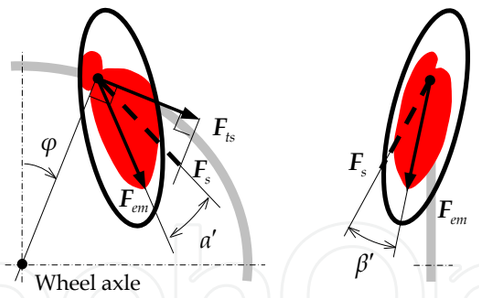

(a) Sagittal plane (b) Frontal plane

Fig. 18. Definition of component and angle of driving force contribution figure.

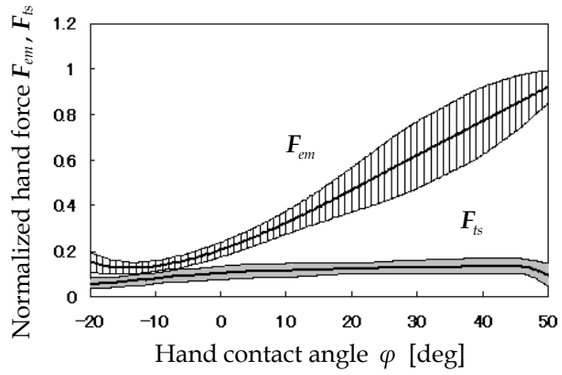

Fig. 19. Maximum driving force F_{em} and tangential component of measured hand force F_s to the handrim F_{ts}.

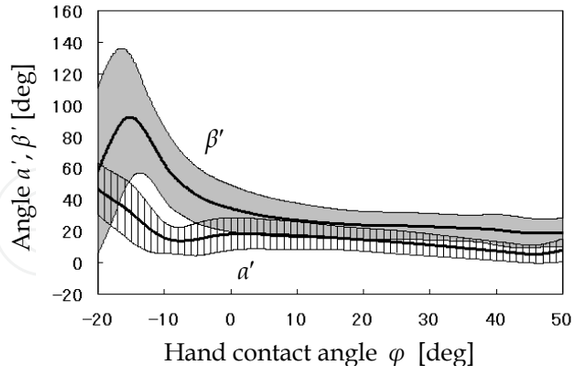

Fig. 20. Angle between F_{em} and measured hand force F_s.

5.4 Optimal Wheelchair Design

As described above, we performed analyses of wheelchair maneuverability quantitatively from the viewpoint of upper limb manipulability. The analytical results show that wheelchair users start driving the handrim in such a posture that it is difficult to generate the necessary hand force to drive the wheelchair. This might be a problem of wheelchairs,

and might be a cause of the increased physical load borne by wheelchair users. Using a new concept of the driving force contribution figure reflecting the driving efficiency to the manipulating force ellipsoid, the results accurately characterize wheelchair users driving the wheelchair, with consideration of the upper limb load and wheelchair propulsion efficiency.
The design and the adaptation of the wheelchair have generally been performed using trial and error based on experience and knowledge acquired over many years. However, their grounds and effects remain unclear. The wheelchair design criteria and evaluation of the adaptability between users and designed wheelchairs have not been established.
The proposed methods are useful not only for the quantitative evaluation of upper limb manipulability based on individuals' joint torque characteristics but also for prediction of the hand force pattern taken for the given task that the user must perform. In addition, for optimal wheelchair design, we have been developing other evaluation methods (Miura et al., 2004, 2006; Sasaki et al., 2008) including the estimation of physical loads using an upper limb musculoskeletal model, optimization of the driving form using genetic algorithms, and development of a wheelchair simulator that can freely adjust wheelchair dimensions according to the user's body functions. Therefore, using the evaluation methods proposed in this chapter or by combining them with other optimization methods we have developed, we can reasonably provide individually adjusted wheelchairs that reduce the physical load on users' upper limbs during wheelchair propulsion and which increase the wheelchair propulsion efficiency.

6. Conclusion

This chapter has presented a manipulating force ellipsoid and polytope based on human joint torque characteristics for evaluation of upper limb manipulability. As described in sections 3 and 4, the proposed methods are based on the relation between the joint torque space and the hand force space. Therefore, it is certain that more accurate evaluation can be achieved by expanding these concepts and by considering the relations among muscle space, joint torque space, and hand force space. However, the development of the three-dimensional musculoskeletal model of the human is a respected research area in the field of biomechanics. It is difficult to model the individual's muscle properties strictly, such as the maximum contraction force, the origin, the insertion and the length of each muscle. Because of this fact, the proposed evaluation method is a realistic technique by which the influence of the remaining muscle strength or paralysis can be modeled directly and easily as the individual's joint torque characteristics. Nevertheless, further improvements are necessary to achieve a more accurate evaluation because the bi-articular muscle characteristics cannot be reflected sufficiently using the method of separately measuring the maximum joint torque characteristics of each joint.
Through our investigations, we have solved three problems to express the manipulating force ellipsoid and polytope based on the measured maximum joint torque. The first is to have reflected the human joint torque characteristics depending on the joint angle and the rotational direction into the formulation of the manipulating force ellipsoid and polytope. Here, the peculiar feature of humans, that the region of maximum joint torque is not symmetric about the origin, was expressed by introducing the offset between the origin of the ellipsoid and the hand position. The second is to have derived two visualization methods of higher-dimensional hyperellipsoids such as the orthogonal projection and the

section, to evaluate the upper limb manipulability quantitatively and visually. Furthermore, the third is to have derived a new vertex search algorithm for higher-dimensional polytopes to search for all vertexes of convex polytopes without oversight by an easy calculating formula and few computational complexities. It is certain that the proposed methods are effective not only for evaluation of the manipulability of human upper limbs but also for the evaluation of a robot manipulator's manipulation capability because no reports, even in the robotics literature, have described solutions to these problems. Therefore, the proposed methods can probably contribute to progress in the field of robotics in a big way, offering useful new findings.

In this chapter, the analysis of the wheelchair propulsion was introduced as one example to evaluate the proposed methods' practical importance. In addition, the potential problems of wheelchairs and the wheelchair maneuverability were clarified quantitatively from the viewpoint of the upper limb manipulability. Results described herein show that the ease of hand force manipulation engenders improvement in all scenes of daily living and yields various new findings. Especially, it is important to evaluate upper limb manipulability of elderly and physically handicapped people quantitatively and visually for development of assistive devices, planning of rehabilitation, and improvement of living environments. Further applications of the proposed methods as a new evaluation index for the manipulability analysis of upper and lower limbs in various fields, including ergonomics and robotics, can be anticipated.

7. Acknowledgements

The authors gratefully acknowledge the support provided for this research by a Japan Society of Promotion of Science (JSPS) Grant-in-Aid for Young Scientists (Start-up 18800034 and B 20700463).

8. References

Ae, M.; Tang, H.P. & Yokoi, T. (1992). Estimation of inertia properties of the body segments in Japanese athletes, In: *Biomechanism*, Vol. 11, pp. 23–32, The Society of Biomechanisms Japan, ISBN 978-4-13-060132-0.

Asada, H. & Slotine, J.-J.E. (1986). *Robot Analysis and Control*, John Wiley and Sons, ISBN 0-471-83029-1.

Chiacchio, P.; Bouffard-Vercelli, Y. & Pierrot, F. (1997). Force polytope and force ellipsoid for redundant manipulators. *Journal of Robotic Systems*, Vol. 14, No. 8, pp. 613–620, ISSN 0741-2223.

Cooper, R.A. (1998). *Wheelchair selection and configuration*, Demos Medical Publishing, ISBN 1-888799-18-8.

Engstrom, B. (2002). *Ergonomic seating. A true challenge. Wheelchair seating & mobility principles*, Posturalis Books, ISBN 91-972379-3-0.

Gellman, H.; Chandler, D.R.; Petrasek, J.; Sie, I.; Adkins, R. & Waters, R.L. (1988). Carpal tunnel syndrome in paraplegic patients. *The Journal of Bone and Joint Surgery*, Vol. 70, No. 4, pp. 517–519, ISSN 0021-9355.

Hamada, Y.; Joo, S-W. & Miyazaki, F. (2000). Optimal design parameters for pedaling in man–machine systems. *Transactions of the Institute of Systems, Control and Information Engineers*, Vol. 13, No. 12, pp. 585–592, ISSN 1342-5668.

Lee, J. (2001). A structured algorithm for minimum l∞-norm solutions and its application to a robot velocity workspace analysis. *Robotica*, Vol. 19, pp. 343–352, ISSN 0263-5747.

Miura, H.; Sasaki, M.; Obinata, G.; Iwami, T.; Nakayama, A.; Doki, H. & Hase, K. (2004). Task based approach on trajectory planning with redundant manipulators, and its application to wheelchair propulsion, *Proceedings of the 2004 IEEE Conference on Robots, Automation and Mechatronics*, pp. 758–761, Singapore, ISBN 0-7803-8645-0.

Miura, H.; Sasaki, M.; Obinata, G.; Iwami, T. & Hase, K. (2006). Three-dimensional Motion Analysis of Upper limb for Optimal Design of Wheelchair, In: *Biomechanisms*, Vol. 18, pp. 89–100, The Society of Biomechanisms Japan, ISBN 4-7664-1305-9.

Miyawaki, K.; Iwami, T.; Obinata, G.; Kondo, Y.; Kutsuzawa K.; Ogasawara, Y. & Nishimura, S. (2000). Evaluation of the gait of elderly people using an assisting cart: gait on flat surface. *JSME International Journal, Series C*, Vol. 43, No. 4, pp. 966–974, ISSN 1344-7653.

Miyawaki, K.; Iwami, T.; Ogasawara, Y.; Obinata, G. & Shimada, Y. (2007). Evaluation and development of assistive cart for matching to user walking. *Journal of Robotics and Mechatronics*, Vol. 19, No. 6, pp. 637–645, ISSN 0915-3942.

Ohta, K.; Luo, Z. & Ito, M. (1988). Analysis of human movement under environmental constraints: Adaptability to environment during crank rotation tasks. *Transactions of the Institute of Electronics, Information and Communication Engineers*, Vol. J81-D-II, No. 6, pp. 1392–1401, ISSN 0915-1923.

Oikawa, K. & Fujita K. (2000). Algorithm for calculating seven joint angles of upper extremity from positions and Euler angles of upper arm and hand. *Journal of the Society of Biomechanisms*, Vol. 24, No. 1, pp. 53–60, ISSN 0285-0885.

Oshima, T.; Fujikawa, T. & Kumamoto, M. (1999). Functional evaluation of effective muscle strength based on a muscle coordinate system consisted of bi-articular and mono-articular muscles: contractile forces and output forces of human limbs. *Journal of the Japan Society for Precision Engineering*, Vol. 65, No. 12, pp. 1772–1777, ISSN 0912-0289.

Pentland, W.E. & Twomey, L.T. (1994). Upper limb function in persons with longterm paraplegia and implications for independence: part I. *Paraplegia*, Vol. 32, pp. 211–218, ISSN 0031-1758.

Sasaki, M.; Iwami, T.; Miyawaki, K.; Doki, H. & Obinata, G. (2004). Three-dimensional spatial expression of the manipulability of the upper limb considering asymmetry of maximum joint torque. *Transactions of the Japan Society of Mechanical Engineers, Series C*, Vol. 70, No. 697, pp. 2661–2667, ISSN 0387-5024.

Sasaki, M.; Iwami, T.; Obinata, G.; Doki, H.; Miyawaki, K. & Kinjo, M. (2005). Biomechanics analysis of the upper limb during wheelchair propulsion. *Transactions of the Japan Society of Mechanical Engineers, Series C,* Vol. 71, No. 702, pp. 654–660, ISSN 0387-5024.

Sasaki, M.; Iwami, T.; Miyawaki, K.; Obinata, G.; Sato, I.; Shimada, Y. & Kiguchi, K. (2007a). A study on evaluation of the manipulability of the upper limb using convex polyhedron: First report, new vertex search algorithm. *Transactions of the Japan Society of Mechanical Engineers, Series C,* Vol. 73, No. 729, pp. 1514–1521, ISSN 0387-5024.

Sasaki, M.; Iwami, T.; Obinata, G.; Miyawaki, K.; Miura, H.; Shimada, Y. & Kiguchi, K. (2007b). Analysis of wheelchair propulsion and hand force pattern based on manipulability of the upper limb. *Transactions of the Japan Society of Mechanical Engineers, Series C,* Vol. 73, No. 732, pp. 2279–2286, ISSN 0387-5024.

Sasaki, M.; Kimura, T.; Matsuo, K.; Obinata, G.; Iwami, T.; Miyawaki, K. & Kiguchi, K. (2008). Simulator for optimal wheelchair design. *Journal of Robotics and Mechatronics*, Vol. 20, No. 6, pp. 854–862, ISSN 0915-3942.

Shim, I.C. & Yoon, Y.S. (1997). Stabilization constraint method for torque optimization of a redundant manipulator, *Proceedings of the 1997 IEEE International Conference on Robotics and Automation*, pp. 2403–2408, ISBN 0-7803-3612-7, Albuquerque, NM, April, 1997.

Sie, I.H.; Waters, R.L.; Adkins, RH & Gellman, H. (1992). Upper extremity pain in the postrehabilitation spinal cord injured patient. *Archives of Physical Medicine and Rehabilitation*, Vol. 73, pp. 44–48, ISSN 0003-9993.

Trudel, G.; Kirby, R.L. & Bell, A.C. (1995). Mechanical effects of rear-wheel camber on wheelchairs. *Assistive Technology*, Vol. 7, No. 2, pp. 79–86, ISSN 1040-0435.

Yoshikawa, T. (1984). Analysis and control of robot manipulators with redundancy, In: *Robotics Research: The First International Symposium of Robotics Research*, Brady, M. & Paul, R. (Ed.), pp. 735–747, MIT Press, ISBN 0-262-52392-2.

Yoshikawa, T. (1985). Dynamic manipulability of robot manipulators. *Journal of Robotic Systems*, Vol. 2, pp. 113–124, ISSN 0741-2223.

Yoshikawa, T. (1990). *Foundations of Robotics: Analysis and Control*, MIT Press, ISBN 0-262-24028-9.

Robot Manipulators New Achievements

Edited by Aleksandar Lazinica and Hiroyuki Kawai

ISBN 978-953-307-090-2
Hard cover, 718 pages
Publisher InTech
Published online 01, April, 2010
Published in print edition April, 2010

Robot manipulators are developing more in the direction of industrial robots than of human workers. Recently, the applications of robot manipulators are spreading their focus, for example Da Vinci as a medical robot, ASIMO as a humanoid robot and so on. There are many research topics within the field of robot manipulators, e.g. motion planning, cooperation with a human, and fusion with external sensors like vision, haptic and force, etc. Moreover, these include both technical problems in the industry and theoretical problems in the academic fields. This book is a collection of papers presenting the latest research issues from around the world.

InTech Europe
University Campus STeP Ri
Slavka Krautzeka 83/A
51000 Rijeka, Croatia
Phone: +385 (51) 770 447
Fax: +385 (51) 686 166
www.intechopen.com

InTech China
Unit 405, Office Block, Hotel Equatorial Shanghai
No.65, Yan An Road (West), Shanghai, 200040, China
中国上海市延安西路65号上海国际贵都大饭店办公楼405单元
Phone: +86-21-62489820
Fax: +86-21-62489821

IntechOpen